Remote Sensing of Environment 144 (2014) 1–10

Contents lists available at ScienceDirect

Remote Sensing of Environment

journal homepage: www.elsevier.com/locate/rse

# Freeboard and mass extraction of the disintegrated Mertz Ice Tongue with remote sensing and altimetry data

Xianwei Wang [a,b,c,*], Xiao Cheng [a], Peng Gong [d,e], C.K. Shum [a,c], David M. Holland [b], Xiaowen Li [a]

[a] State Key Laboratory of Remote Sensing Science, and College of Global Change and Earth System Science, Beijing Normal University, Beijing 100875, China
[b] Center for Global Sea Level Change, New York University Abu Dhabi, Abu Dhabi, United Arab Emirates
[c] Division of Geodetic Science, School of Earth Sciences, The Ohio State University, OH 43210, USA
[d] Ministry of Education Laboratory Key Laboratory for Earth System Modeling, and Center for Earth System Science, Tsinghua University, Beijing 100084, China
[e] Department of Environmental Science, Policy and Management, University of California, Berkeley, CA 94720-3114, USA

ARTICLE INFO

*Article history:*
Received 17 July 2013
Received in revised form 14 January 2014
Accepted 15 January 2014
Available online 31 January 2014

*Keywords:*
Freeboard
Ice thickness
ICESat
Remote sensing
Mertz Ice Tongue

ABSTRACT

In February 2010, the Mertz Ice Tongue (MIT) collapsed and generated a giant iceberg. However, parameters about this iceberg have not been calculated and published in detail. In this study, the freeboard map of this iceberg was generated for the first time using a time-series ICESat/GLAS data. Methods for producing the freeboard map of this iceberg are suggested. Field data for ice velocity were used to relocate the footprints collected by different campaigns. Cross-validation was conducted with freeboards extracted from crossovers observed within 30 days of each other. The precision of the freeboard extraction is approximately ±0.50 m, when taking one standard deviation as the precision. The freeboard varied from 23 m to 59 m with the mean of 41 m. With assumption of hydrostatic equilibrium (assuming a snow layer depth of 1 m, a snow density of 360 kg/m$^3$, an ice density of 915 kg/m$^3$ and a sea water density of 1024 kg/m$^3$), the minimum, maximum and average ice thickness were calculated as 210 m, 550 m and 383 m respectively. The total ice loss is approximately $8.96 \times 10^{11}$ tons over an area, 34 km in width and 75 km in length, or approximately 2560 ± 5 km$^2$. These parameters extracted from remote sensing and altimetry data will provide additional information for studies of the evolution of iceberg, especially in iceberg tracking system.



## 1. Introduction

Antarctica is the earth's largest ice storage base, containing approximately 88% of the earth's ice mass (Allison, Alley, Fricker, Thomas, & Warner, 2009). Because of their complex links to climate change and direct effects on sea level changes, Antarctic ice changes are of great interests to many researchers (Alley, Clark, Huybrechts, & Joughin, 2005; Zwally et al., 2005). Floating ice shelves and calving outlet glaciers are primary sites of mass loss (Allison et al., 2009). Large icebergs can be generated if ice shelves collapse or disintegrate, as occurred at Larsen A, Larsen B, Wilkins and Mertz Ice Shelves in 1995, 2002, 2008 and 2010, respectively (Cook & Vaughan, 2010; Lescarmontier et al., 2012; Scambos, Hulbe, Fahnestock, & Bohlander, 2000; Scambos, Sergienko, Sargent, MacAyeal, & Fastook, 2005; Scambos et al., 2009). Icebergs play critical roles in many geophysical and biological processes, affecting ship route planning and directly influencing local weather forecasting (Arrigo & van Dijken, 2003; Arrigo, van Dijken, Ainley, Fahnestock, & Markus, 2002; Stuart & Long, 2011). Because of the critical role of icebergs, an automatic iceberg tracking method based on image segmentation technology using Landsat, MODerate-resolution Imaging Spectroradiometer (MODIS) and Huan Jing (HJ) 1B data was proposed by Zhao, Liu, and Gong (2012). An Antarctic iceberg tracking system that uses SeaWinds (a microwave scatterometer) data to deduce the routes of icebergs was built by Stuart and Long (2011). Aside from these geographical locations, however, many other parameters about icebergs, such as their area, freeboard or thickness, remain unmeasured because of the limited use of data by the iceberg tracking system to make these observations.

Remote sensing technology has long been used to identify land-based features. Both microwave and optical sensors such as Envisat-Advanced Synthetic Aperture Radar (ASAR), Radarsat, Landsat, Système Pour l'Observation de la Terre(SPOT), QuickBird and others (Bindschadler, 2002; Fricker, Young, Allison, & Coleman, 2002; Løset & Carstens, 1996; Paul et al., 2013; Scheuchl, Flett, Caves, & Cumming, 2004), have been used for studies of ice change. The area of specific land covers or objects can be measured precisely with the high-resolution images provided by these satellites. However, for ice shelf and iceberg detection, because of the frequent bad weather in the polar regions, microwave sensors are recommended due to their ability to penetrate cloud cover (Stuart & Long, 2011). The freeboard of sea ice in both the Southern and Arctic Oceans was successfully extracted using altimetry data, especially laser altimetry data (Farrell, Laxon, McAdoo, Yi, & Zwally, 2009; Farrell et al., 2012; Forsberg & Skourup, 2005; Kurtz et al., 2008; Kwok & Cunningham, 2008; Kwok, Cunningham, Zwally, & Yi, 2006, 2007; Laxon, Peacock, & Smith, 2003; Laxon et al., 2013; Yi, Zwally, &

* Corresponding author.
*E-mail address:* wangxianwei0304@163.com (X. Wang).

0034-4257/$ – see front matter © 2014 Elsevier Inc. All rights reserved.
http://dx.doi.org/10.1016/j.rse.2014.01.002

Robbins, 2011; Zwally, Yi, Kwok, & Zhao, 2008). Additionally, ice thickness can be estimated from freeboard data or draft data by assuming hydrostatic equilibrium (Wang et al., 2011). Estimation of ice thickness data is more difficult and has larger uncertainties.

In general, to fully understand the evolution of icebergs, more parameters must be measured with remote sensing techniques. Providing more iceberg parameters for iceberg tracking systems would benefit scientists across multiple disciplines. Oceanographers could predict the heat and salinity exchange more accurately between iceberg and ocean water with models (Ardhuin, Tournadre, Queffeulou, Girard-Ardhuin, & Collard, 2011; Martin, Drucker, & Kwok, 2007) or its effect to sea ice area and thickness in vicinity of iceberg (Martin & Adcroft, 2010). Glaciologist could reveal the revolution of iceberg more completely by comparing the different parameters observed at different times (Silva & Bigg, 2005), evaluate its effect to ship route and avoid the collisions with ships. Ecologists and Biogeochemists could evaluate the effect to phytoplankton decline or bloom with more specific parameters of icebergs (Arrigo et al., 2002; Schwarz & Schodlok, 2009; Vernet, Sines, Chakos, Cefarelli, & Ekern, 2011). Geochemists could better understand the sediment transport, potential iron flux or carbon export caused by icebergs (Lin, Rauschenberg, Hexel, Shaw, & Twining, 2011; Smith et al., 2011).

In this paper, we use Mertz Ice Shelf as an example to measure parameters from a disintegrated section of it using remote sensing imagery and a time-series of laser altimetry data, including area, freeboard map, ice thickness and ice mass. The method of producing the freeboard map production for the iceberg before disintegration is suggested. The ice thickness and ice mass were calculated with a time-series of ICESat/GLAS data.

## 2. Mertz Ice Tongue

The Mertz Ice Shelf (66°S–68°S, 144°E–150°E) (Fig. 1) is located in King George V Land, East Antarctica (McMullen et al., 2006; Wendler, Ahlnas, & Lingle, 1996), which drains approximately 83,000 km$^2$ of the grounded East Antarctica Ice Sheet (Rignot & Jacobs, 2002). The ice tongue extends over 140 km from its grounding line to the shelf front and has a width of approximately 30 km at the front (Legresy, Wendt, Tabacco, Remy, & Dietrich, 2004). The ice velocity here is fast, more than 1 km/a (Rignot, Mouginot, & Scheuchl, 2011; Wang, 2012; Wendler et al., 1996), which drains ice at approximately 16.4 Gt/a (Berthier, Raup, & Scambos, 2003). Interdisciplinary research has been performed on the MIT. For example, the tidal currents around the MIT were studied by Legresy et al. (2004) with Global Position System (GPS) data and remote sensing data; they detected a flexure of up to 2 m per day. Based on Interferometric Synthetic Aperture Radar (InSAR) data acquired in 1996, Rignot and Jacobs (2002) calculated a basal melting rate of 17 ± 6 m/a on the Mertz Glacier in the vicinity of its grounding line. Roberts, Allison, and Lytle (2001) also studied the sensible- and latent-heat-fluxes over the Mertz Glacier polynya using atmospheric data collected in August, 1999. These data suggested a high sea ice production rate there. The interaction between multi-year fast ice and the MIT was detected with altimetry and remote sensing data and the influence of multi-year sea ice on the MIT was confirmed by Massom et al. (2010). Rift propagation on the MIT before its disintegration was measured with GPS data by Lescarmontier et al. (2012).

On February 12 or 13, 2010, a large iceberg calved from the MIT after the B9B ice berg (Tamura, Williams, Fraser, & Ohshima, 2012) collided with the ice shelf. This event triggered multiple changes in this region, including sea ice production changes and phytoplankton blooms (Pyper, Rintoul, Tilbrook, & van Wijk, 2011). Tamura et al. (2012) found that the sea ice production for the Mertz Glacier region decreased from 144 km$^3$ in 2000 to 134 km$^3$ in 2011 after the calving because the calving decreased polynya activity. The disintegrated iceberg was reported with an averaged thickness of approximately 400 m and area of approximately 2500 km$^2$ (http://www.sciencedaily.com/releases/2010/02/100226112732.htm). The detailed freeboard, ice thickness

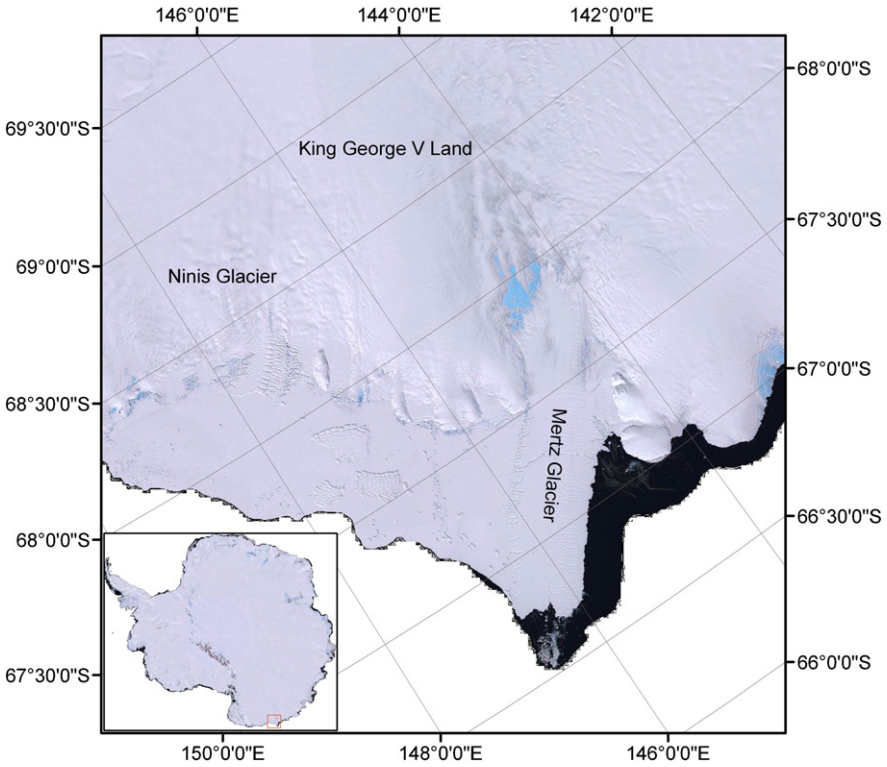


**Fig. 1.** Location of Mertz Ice Shelf in East Antarctica (Wang, 2012). (Red square indicates the location of Mertz Ice Shelf in Antarctica ice sheet and the background is MODIS Mosaic of Antarctica with a resolution of 250 m. Regions in white are oceans).

and ice mass of this iceberg were not measured or provided, even in the iceberg tracking system.

## 3. Data

### 3.1. ICESat data

The Ice, Cloud, and Land Elevation Satellite (ICESat) was the first laser altimeter satellite to orbit the earth (Schutz, Zwally, Shuman, Hancock, & DiMarzio, 2005; Zwally et al., 2002). It did so from March 2003 to October 2009. With three Geoscience Laser Altimeter System (GLAS) sensors onboard, ICESat/GLAS has carried out 19 campaigns in which it provided vital observations for snow, ice and land change research (Wang et al., 2011) and 15 different types of data were produced for scientific uses. The reported precision and accuracy of its altimetry are approximately 2 cm and 14 cm, respectively (Shuman et al., 2006). The pointing error in the horizontal direction is approximately 6 m (Abshire et al., 2005). Its footprint is approximately 70 m in diameter, which is much smaller than that of radar altimeters (Wang et al., 2011). ICESat/GLAS operated at a working frequency of 40 Hz and the distance between two adjacent footprints was approximately 170 m. Its denser along-track footprints, the higher accuracy of altimetry and its smaller footprints compensate for the shortcomings of other radar altimeters and make it widely used in various fields (Wang, 2012; Wang, Cheng, Huang, & Li, 2013; Wang, Gong, et al., 2013).

In this study, GLA12 data covering the MIT from 2003 to 2009 were used. Fig. 2 shows the distribution of these data. It shows that several tracks cover the MIT (T46, T188, T165, T31, T1170, T307, T1147 and T1289). The red polygon in Fig. 2 shows the buffer area of the boundary of the Mertz Ice Shelf in 2007 from ASAR WSM data, with 10 km as the buffer radius. ICESat/GLAS data fallen in this region were chosen for subsequent calculations.

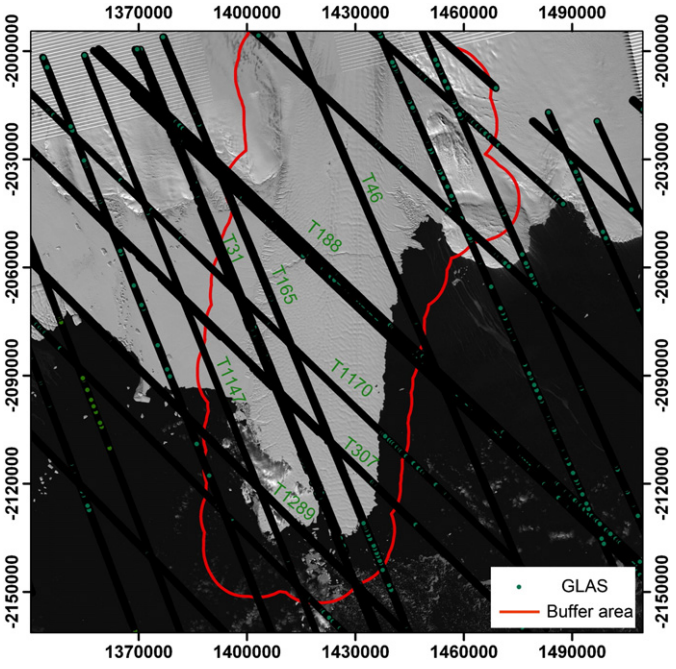


**Fig. 2.** Locations of ICESat/GLAS footprints on MIT. The green dot with black boundary indicates the ICESat/GLAS footprint. The red polygon is the buffer region of boundary of Mertz Ice Shelf, with 10 km as buffer radius. The ice shelf boundary was derived in 2007.

### 3.2. Landsat data

Landsat is a series of earth-observing satellite missions jointly managed by the National Aeronautics and Space Administration (NASA) and the United States Geological Survey (USGS). It has been operating since 1972. The Thematic Mapper (TM) and the Enhanced Thematic Mapper Plus (ETM+) have been used as the primary imaging sensors. The resolution is approximately 30 m for multiple spectrum bands, from visible to middle-infrared and 15 m for the panchromatic band of Landsat 7 (Arvidson, Gasch, & Goward, 2001). Landsat 7 is currently in operation; however, in May 2003, its Scan Line Corrector (SLC) was damaged, resulting in data gaps in images captured by Landsat 7 (Maxwell, Schmidt, & Storey, 2007). On February 11, 2013, Landsat 8 was launched successfully (http://landsat.usgs.gov/LDCM_Landsat8.php). These satellites provide many images useful for scientific research. The high resolution of the panchromatic band of Landsat 7 makes it suitable for area-change detection. Because of the effective coverage in the MIT region and their high resolution, images from Landsat 7 were used to calculate the area of the disintegrated iceberg (Figs. 2, 4 and 5).

## 4. Methods

### 4.1. Extraction of freeboard

The freeboard calculation method has been discussed by Zwally et al. (2008), Kwok et al. (2006), Kwok et al. (2007), Kwok and Cunningham (2008) and Wang et al. (2011). They identified sea level extraction as the most critical step in the method. In this section, multiple time-series of ICESat/GLAS data were preprocessed and then relocated for subsequent calculations. Next, sea level was identified from other footprints in the same tracks. Finally, freeboard was calculated and edited to produce a freeboard map of the MIT.

#### 4.1.1. Preprocessing of ICESat/GLAS data

Corrections for the instrument, the moisture content of the troposphere and the tides were applied during the processing of ICESat surface elevation data (Zwally et al., 2008). Elevation field in the GLA12 data named as *i_elev* is the primary elevation data. The elevation in the GLA12 release-33 data file contains ocean tide corrections from TPX07.1 tide model. However, our analysis requires the instantaneous sea surface condition to calculate the sea level height. According to Phillips, Ridgway, Minster, Yi, and Bentley (1999), the magnitude of the tidal correction on the ice shelf and coast are approximately $\pm 1$ m and $\pm 2$ m with uncertainties of approximately $\pm 0.40$ m and $\pm 0.10$ m respectively. Thus, the tidal correction should be removed (Farrell et al., 2012) from the ICESat elevation field.

The saturation correction, however, is not included in *i_elev*. Thus, a saturation correction *i_satElevCorr* should be added to *i_elev* to obtain the corrected elevation (Wang, Gong, et al., 2013; Wang et al., 2012). For GLA12 data, the processed elevation (*Pro_elev*) can be obtained from Eq. (1).

$$Pro\_elev = i\_elev + i\_satElevCorr + i\_ocElv + i\_ldElv - i\_gdHt \quad (1)$$

where *i_elev* is the elevation, *i_satElevCorr* is the saturation elevation correction, *i_gdHt* is the geoid height from the EGM-08 model, *i_ocElv* is the ocean tidal elevation and *i_ldElv* is the load tidal elevation from the GLA12 data files.

#### 4.1.2. Relocation of footprints

Because of the large ice velocity on MIT, footprints observed at different times cannot be compared to one another. For example, the ice observed in 2003 by ICESat/GLAS flowed downstream to a new position by 2009. Thus, the footprints observed by earlier campaigns must be relocated. An ice velocity map of MIT with a resolution of approximately

900 m was obtained from Rignot et al. (2011) who produced it using the InSAR method. The InSAR data are from ALOS PALSAR data acquired from 2006 to 2010. This time period overlaps well with the period of ICESat observation, from 2003 to 2009. Over this period, the ice shelf was stable and the velocity relatively constant, so we assume a constant ice velocity over this period. Oct. 1, 2009, was the last day of that ICESat/GLAS data taken in this region so we chose this as a standard date around which to relocate the footprints. All footprints observed before this data are adjusted. Thus the location could be adjusted with Eq. (2).

$$X = x + \int_{t_1}^{t_2} v_x dt$$
$$Y = y + \int_{t_1}^{t_2} v_y dt \quad (2)$$

where, $x$ and $y$ are location in the $X$ and $Y$ directions, respectively; $v_x$ and $v_y$ are the ice velocity in the $X$ and $Y$ directions respectively; $t_1$ is the start time, and $t_2$ is the end time. In calculations with actual data, the integral was replaced by a sum, thus transforming Eq. (2) to Eq. (3).

$$X = x + \sum_{i=1}^{n} v_{xi}\Delta t + v_x(t_2 - t_1 - n\Delta t)$$
$$Y = y + \sum_{i=1}^{n} v_{yi}\Delta t + v_y(t_2 - t_1 - n\Delta t) \quad (3)$$

where $\Delta t$ is the time step, $v_{xi}$ and $v_{yi}$ are the ice velocity in the $X$ and $Y$ directions in time period 'i' respectively, and $n$ is the integer number of total time steps. In this paper, $\Delta t$ was set to 10 days.

#### 4.1.3. Freeboard calculation

Freeboard is defined as the vertical height of the ice shelf or sea ice above sea level. In this paper, the freeboard of MIT contains two parts: ice out of sea water and snow on the top of ice. On MIT, ICESat/GLAS data were processed according to a separated track, where data from the same track were acquired at almost the same time. Determining the sea level height is critical and is usually performed with data from footprints covering leads or thin ice (Wang et al., 2011; Zwally et al., 2008).

The observation with the lowest elevation in the profile was taken to be the footprint presenting the sea level (Fig. 3, footprint marked with a square box). Because of the short length of elevation profiles covering the ocean, the elevation over the footprint was taken as the sea level height in this profile. Freeboard was calculated as follows:

$$H_f = pro\_elev - sea\_level\_Elev \quad (4)$$

where $H_f$ is the freeboard height and *sea_level_Elev* is the elevation of the sea surface.

#### 4.1.4. Freeboard map production

The freeboard calculated along the profile in this region had up to three classes: ice-shelf freeboard, sea-ice freeboard and multi-year-ice freeboard. To separate ice-shelf freeboard from the other two classes, a freeboard threshold was set: footprints with freeboard greater than 17 m were taken as being part of the MIT and were therefore assigned as ice-shelf freeboard.

Fig. 3 shows the elevation profile from track 1170, the location of which was shown in Fig. 2. Local elevation maxima and minima were calculated and revised. There are crevasses on the surface of the MIT, which can cause the terrain anomalies. To avoid these, footprints falling in deep crevasse depth greater than 6 m were excluded from the study. To calculate the crevasse depth, local maxima and minima along the elevation profile were determined and revised. After that, freeboard data on the MIT were used to produce a map with a resolution of 1200 m. The kriging method was used because this method combines all the data and spatial relations around interpolation points to make an unbiased estimate (Heritage, Milan, Large, & Fuller, 2009). Abnormally interpolated data can thus be avoided, and the trend in freeboard variation can be inferred from this dataset.

### 4.2. Extraction of ice area

The MIT disintegrated in February 2010. The Landsat ETM + data acquired on Dec. 3, 2009 over the MIT (Fig. 4) was used to measure the area of the disintegrated iceberg because of all available images, it is the closest in time to the disintegration. First we extract the

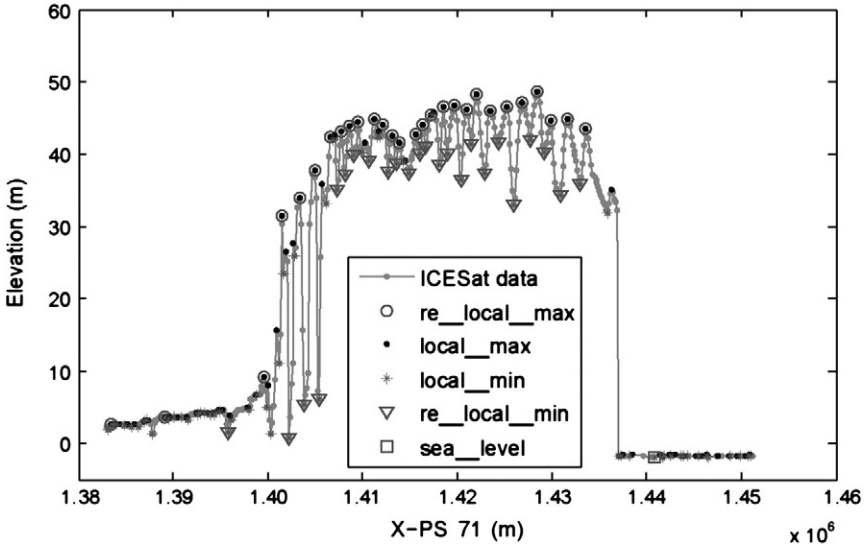


**Fig. 3.** Elevation profile along track 1170. 'local_max' and 'local_min' indicate the local maximum and local minimum of the profile. 're_local_max' and 're_local_min' indicate the revised local maximum and local minimum. 'sea_level' indicates the footprint from the sea surface.

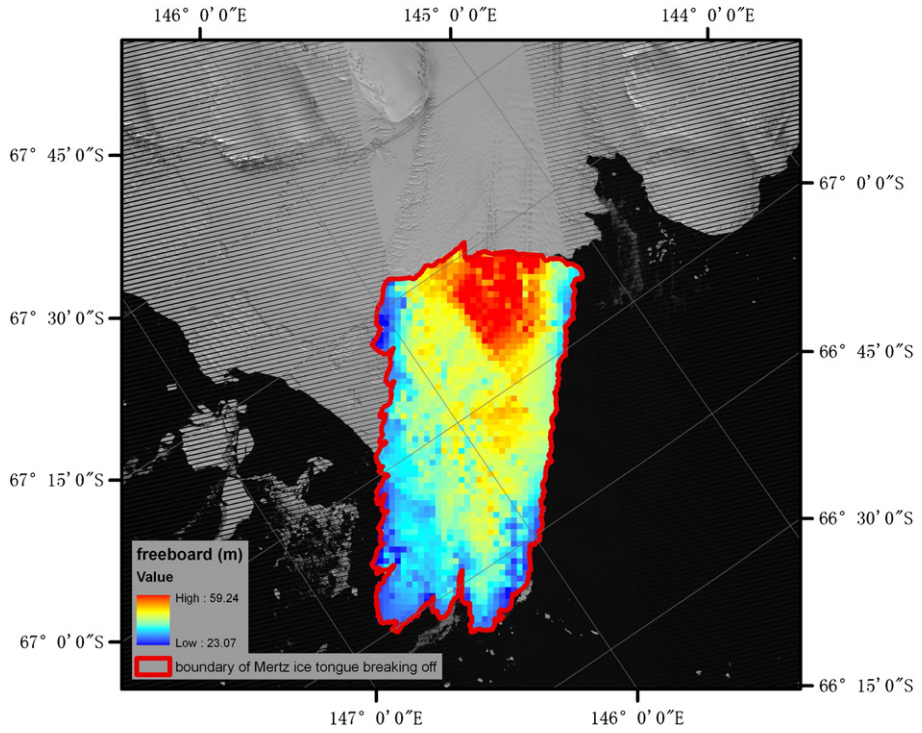


**Fig. 4.** Freeboard map of the disintegrated ice tongue on Mertz Ice Shelf. The background image is from Landsat ETM+ data, captured on Dec. 3, 2009.

panchromatic band with a resolution of 15 m. Then, we translate the data into a Polar Stereographic Projection with −71°S standard latitude. Next we extract the boundary to an ArcGIS shape file manually (red polygon in Fig. 4) using a scale of 1:10,000. The boundary was modified as a linear change over any data gaps in the data. Finally, the area of the polygon was calculated. If one pixel is taken as the uncertainty, our results indicate that, the disintegrated iceberg covers an area of approximately 2560 ± 5 $km^2$. The width and length of this iceberg were measured as approximately 34 km and 75 km respectively.

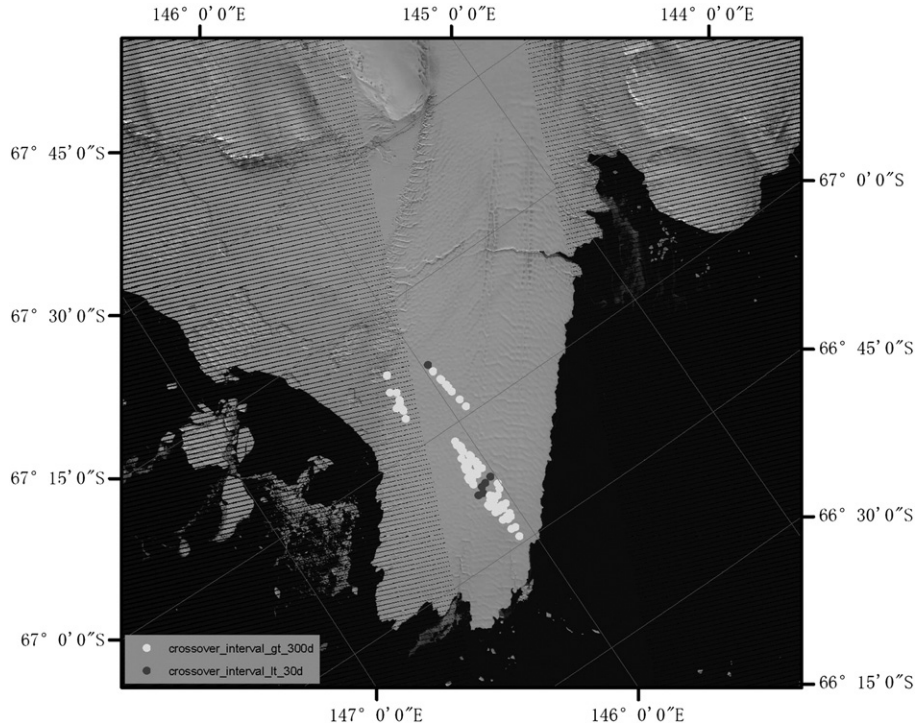


**Fig. 5.** Distribution of crossovers from crossing tracks on the MIT. Gray points and white points indicate the crossovers from tracks observed at the time interval less than 30 days and greater than 300 days respectively. The background image is from Landsat ETM+ data, captured on Dec. 3, 2009.

**Table 1**
Freeboard difference in crossover and averaged region centered at the crossover on MIT. The averaged region is centered in crossover and with a buffer radius of 500 m. '*' and '**' means the freeboard difference from crossover and averaged region respectively.

| Index | X (m) | Y (m) | Start_date (yyyymmdd) | End_date (yyyymmdd) | Interval (d) | Freeboard difference (m)* | Freeboard difference (m)** |
|---|---|---|---|---|---|---|---|
| 1 | 1,409,406 | −2,087,323 | 20031009 | 20031101 | 23 | 0.13 | 0.24 |
| 2 | 1,420,890 | −2,113,687 | 20050615 | 20050606 | 9 | −0.35 | −0.58 |
| 3 | 1,421,309 | −2,111,550 | 20061119 | 20061110 | 9 | 0.06 | 0.04 |
| 4 | 1,419,900 | −2,114,158 | 20040613 | 20040603 | 10 | 0.83 | 0.68 |
| 5 | 1,420,651 | −2,112,461 | 20051116 | 20051106 | 10 | −0.27 | −0.74 |
| 6 | 1,422,338 | −2,110,250 | 20080314 | 20080304 | 10 | −0.00 | −0.03 |

## 5. Validation

### 5.1. Freeboard accuracy

Because of the remoteness, low temperatures and strong winds of the MIT, no in-situ freeboard data are available here. In order to validate the final result calculated in this paper, cross validation was calculated and used as the final precision of the freeboard data. The difference in freeboard between crossovers from two cross tracks (observed at different times) was interpreted as the precision of our result. To reduce the influence of ice motion and variations in the basal melting and surface accumulation between the times of the two observations, only crossovers with in a time difference of 30 days or less were analyzed. Gray points in Fig. 5 show the points used for accuracy validation.

Results from two methods that consider the relocation errors caused by the ice velocity are shown in Table 1. One method uses the freeboard difference in crossover points. The other method uses the averaged freeboard difference over a 500 m region centered on the crossover. As Table 1 indicates, the freeboard difference between crossovers obtained with both methods is relatively small. The average freeboard difference in the crossover point method is approximately 0.07 m, with a standard deviation of ±0.42 m. In the region-averaged method, the average freeboard difference is −0.06 m, with a standard deviation of ±0.52 m. Both methods show almost the same results, which indicates our method extracts stable, high-precision freeboard heights from ICESat/GLAS data.

### 5.2. Rate of changes of freeboard from 2003 to 2009

In order to concentrate on the freeboard changes rather than uncertainty of the freeboard extraction, only freeboards at crossover points from two cross tracks within an observation time interval greater than 300 days were taken as samples. These data are shown as white points in Fig. 5. This selection method yielded 80 crossovers, all of which were used to calculate the rate of change of the freeboard. We show results from both the crossover points and the region-averaged methods described above.

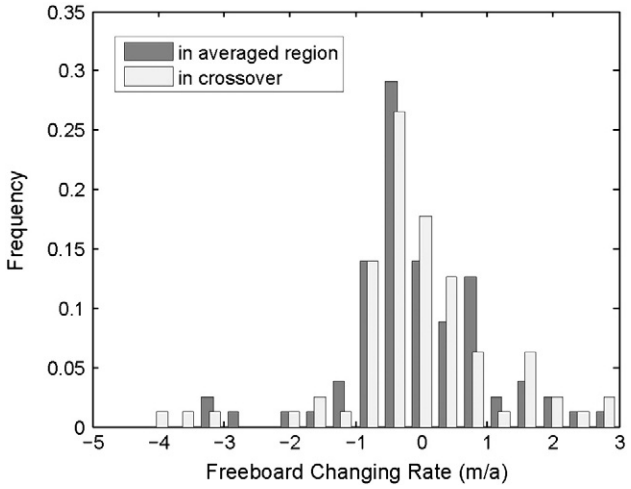


**Fig. 6.** Histogram of changing rate of the freeboard calculated from crossovers and averaged region around crossovers. The averaged region is a buffer region of crossover with 500 m as buffer radius. The interval of changing rate in abscissa is 0.4 m/a.

The histogram of the rate of change in the freeboard calculated from the crossover and region-averaged method are plotted in Fig. 6. The minimum and maximum of the annual rate of change from the crossover point method are −3.89 m/a and 2.91 m/a, respectively, with an annual average rate of change of approximately −0.06 m/a with 1.17 m/a standard deviation. The minimum and maximum of the annual rate of change from the region-averaged method are −3.36 m/a and 2.74 m/a, respectively, with an annual averaged rate of change of approximately −0.07 m/a with 1.06 m/a standard deviation. Histograms of the rates of freeboard change from both methods show the same trend of freeboard variation: there were no obvious changes in freeboard on the MIT from 2003 to 2009. Thus, we conclude that the freeboard there remained unchanged during this time period.

### 5.3. Area of the disintegrated ice tongue

Envisat-ASAR-Wide Swath Mode (WSM) data were also used to extract the area of the disintegrated iceberg. These data had a resolution of approximately 75 m and were acquired on January 9, 2010. The original N1 data were processed with Next European Space Agency SAR Toolbox (NEST) 4C-1.1. After applying image clips, multi-look processing, slant range and ground range transformation, geocoding, projection transformation, boundary extraction and area calculation, we found the final result of the area of the disintegrated iceberg to be 2572 $km^2$. There is slight difference (12 $km^2$) between this and results from Landsat data which finds an area of 2560 $km^2$.

## 6. Discussions

### 6.1. Key points to extract freeboard map

The threshold for excluding footprints that intersect crevasses is set according to statistics of crevasse depth on the MIT. In this way, abnormal changes along the profile were excluded. There is also multi-year sea ice in this region; it has freeboard less than 17 m. The threshold to separate ice-shelf freeboard from sea-ice freeboard and multi-year-sea-ice freeboard was set according to the result from Massom et al. (2010).

When time-series of ICESat/GLAS data are combined, changes in ice location and thickness changes due to surface melting, accumulation and basal melting between different observation times must be considered in freeboard calculation. To adjust the location of footprints, ice velocity data are necessary. Because ice on the MIT moves at approximately 1 km/a, the location of footprints observed on earlier campaigns appears downstream on later campaigns. Thus, footprint relocation is necessary. Furthermore, after relocation, the footprints are distributed evenly on the MIT, which improves interpolation. The freeboard map in Fig. 4 also shows little noise, which may be due to this even pattern in data distribution and the high precision of the freeboard data.

Although the ice velocity data were measured from 2006 to 2010 (Rignot et al., 2011; Wendler et al., 1996), we take the velocity being nearly constant. By comparing the result of freeboard difference at crossover points and over buffer areas around the crossover, we can see that the final result did not change much. Thus an inaccuracy in our assumption of constant ice flow is not obvious and we can conclude that this method of relocating the footprint is effective at making the time-series of data comparable. Similarly, for freeboard changes between different campaigns, the low annual rate of change of freeboard suggested that the freeboard maintained stable over that time. Although we did not consider surface and basal melting, snow accumulation and other effect affecting freeboard in this time period, the freeboard extracted at the different parts of the MIT and different campaigns can be combined since the averaged annual change rate of freeboard from 2003 to 2009 is really small, could be negligible.

Footprints falling in crevasses more than 6 m depth should be excluded to avoid interpolation anomalies in the freeboard map production. As the final freeboard map in Fig. 4 shows, there is an obvious trend in surface elevation over the MIT and little noise. Otherwise, using data from footprints fallen over deep crevasses or region with rift depths greater than 40 m will have obscured the freeboard trend from upstream to downstream and thus would have prevented the use of the kriging method to produce a map.

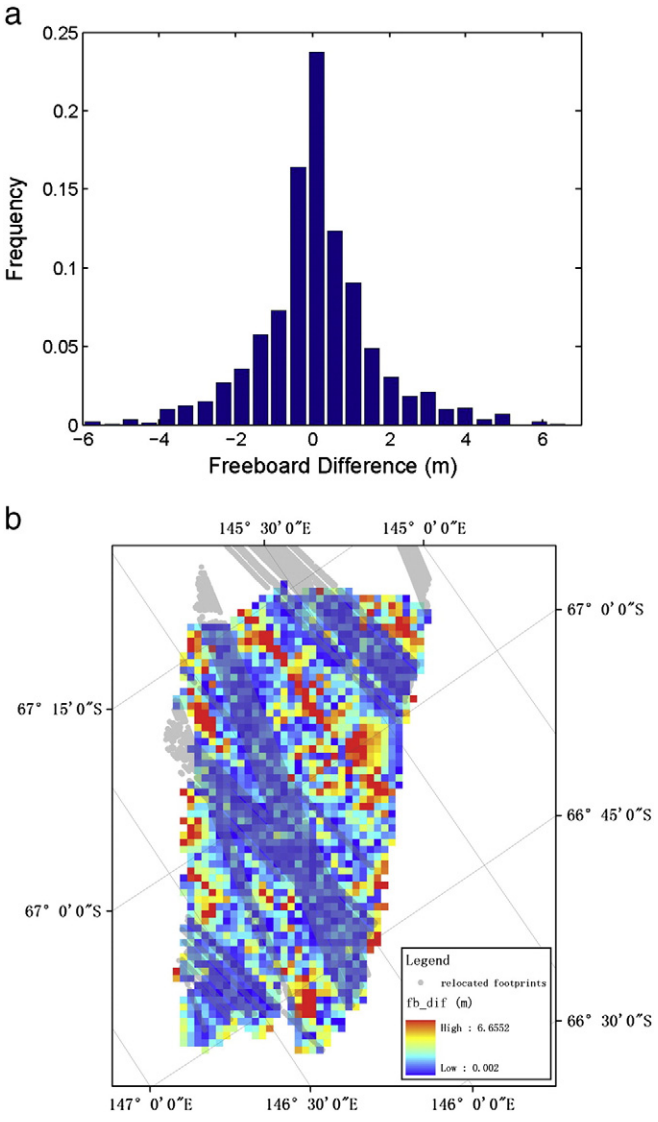


**Fig. 7.** Freeboard comparison with kriging and IDW methods. (a) Histogram of freeboard difference (freeboard from IDW method subtracting that from kriging method). (b): Spatial distribution of absolute value of freeboard difference. The relocated footprints are indicated with gray points.

### 6.2. Freeboard comparison with kriging and inverse distance weighting methods

Both kriging and inverse distance weighting (IDW) methods can be used in generating the digital elevation models. Both methods interpolate values at specific locations using measurements from surrounding locations but differ in way of weight assignment. Many studies have reported the comparison between these methods. In general, kriging is more complicated than IDW and can provide better linear unbiased estimate than IDW (Mueller et al., 2004). Therefore in this paper we adopted the kriging method.

To compare the difference caused by the two interpolation methods, we generated the freeboard map with kriging and IDW methods respectively and calculated the resulting freeboard difference. Fig. 7(a) shows the histogram of freeboard difference. Within 1776 cells, about 79% of the difference fell in the interval from −1.4 m to 1.6 m. The freeboard difference varies from −6.0 m to 6.6 m, with 0.1 m as the mean and 1.5 m as the standard deviation. Thus, on average, freeboard estimates from IDW method are slightly greater than those from kriging, by 0.1 m. Therefore, we could conclude that both methods generate almost the same results when considering the entire freeboard. Freeboard value in each cell may vary by ±1.5 m between the two different methods.

Also from Fig. 7(b), we can find that large difference of freeboard estimates are located almost at the center of data gaps or margins of the MIT, especially from cells in red color. Because of the restriction of track observation of ICESat/GLAS, data collected could not be distributed evenly in space. In vicinity of GLAS measurements, freeboard differences are usually small, which means that both methods have the same effect and the interpolated freeboard is mostly stable. At the center of data gaps, without closer measurements as control, freeboard interpolated by both methods may have low certainty. Additionally, the principal difference of both methods is magnified in these uncertain regions. The ice shelf boundary behaves like cliff, where the freeboard changes suddenly from several tens of meters to zero. Without a sufficient number of footprints covering the boundary region, the interpolation is not stable for either method.

### 6.3. Mass of the disintegrated ice tongue

Fig. 4 shows that freeboard of the iceberg calved from the MIT varies from 23.07 m to 59.24 m, and average 41.39 m. The ice tongue, which is indicated by the red polygon in Fig. 4 is far from the grounding line of the Mertz Ice Shelf. Thus it could be assumed to be floating; that is in hydrostatic equilibrium with the sea water (Berthier et al., 2003; Massom et al., 2001; Wendler et al., 1996). However, additional parameters, such as snow layer depth, snow density, ice density and sea water density are needed to calculate finally the ice thickness. To obtain the ice thickness of the ice tongue, these four parameters were taken as constants, as previous studies have done (Kwok & Cunningham, 2008; Zwally et al., 2008). The ice thickness corresponding to freeboard can be derived from buoyancy theory with Eq. (5).

$$\rho_w \cdot \left(T_i + T_s - H_f\right) = \rho_i \cdot T_i + \rho_s \cdot T_s \tag{5}$$

where $\rho_w$, $\rho_i$ and $\rho_s$ are the densities of ocean water, sea ice and snow respectively; $T_i$ and $T_s$ correspond to ice and snow layer thickness respectively. $H_f$ is the freeboard, from sea surface to the top of the snow layer.

In this paper, the snow layer depth is taken as 1 m, snow density as 360 kg/m$^3$, ice density as 915 kg/m$^3$ and sea water density as

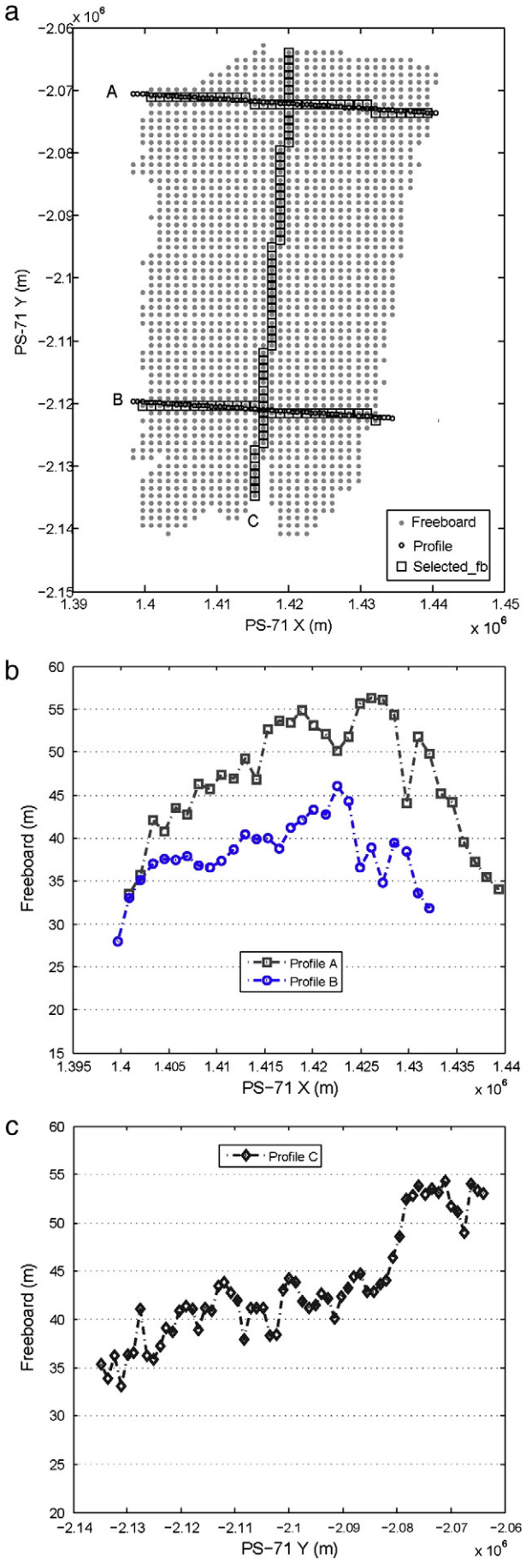


**Fig. 8.** Profile analysis of the freeboard of the disintegrated ice tongue. Two profiles marked A and B are perpendicular to the ice flow direction. Profile C is along the ice flow direction. In (a), the square marked the selected freeboard points. (b) is the freeboard profile in A and B. (c) is the profile in C. In (c), the ice flow direction is from right to left.

1024 kg/m$^3$. With these parameters, the ice thickness $T_i$ will be solved from Eq. (6).

$$T_i = 9.39H_f—6.09 \quad (6)$$

The calculated ice thickness varies from 210.5 m to 550.2 m, and average 382.6 m. These numbers do not include the thickness of snow layer. Considering snow and ice together, the total ice loss of the MIT from the calving event is approximately $8.96 \times 10^{11}$ tons, consisting of $9.2 \times 10^8$ tons of snow and $8.95 \times 10^{11}$ tons of ice. Given the global ocean area of approximately $3.62 \times 10^8$ km$^2$, this is equivalent to approximately 2.4 mm of global sea level. Although the floating ice shelf does not contribute to sea level rise, the continued draining of ice from the Mertz Glacier will transfer more ice into the ocean and contribute to sea level changes.

### 6.4. Terrain analysis of the disintegrated ice tongue

Two profiles (A and B) of freeboard perpendicular to ice flow and one profile (C) parallel to ice flow are plotted in Fig. 8. Fig. 8(a) shows the location of the profile and Fig. 8(b) and (c) shows freeboard within a distance of 600 m from the profile. In the profiles A and B (Fig. 8b), the freeboard on the left side is lower than that on the right side, especially for profile B. This may be caused by different sea ice conditions on each side. On the left side, there is multi-year sea ice (Massom et al., 2010) which interrupted the collapse of the ice shelf. Instead of collapsing, the boundary of the MIT close to the sea ice became thinner, but stayed connected to the MIT. On the right side, there is a polynya that did not freeze over, even in austral winter. The thinning boundary may not stay attached to the MIT and may disintegrate with the influence of the tide, the wind and the circular Antarctic current. The remote sensing imagery also indicates a more orderly boundary on the right side than on the left side, which may be primarily caused by these factors.

Fig. 8(c) shows that the freeboard decreased downstream on MIT. The average slope of this profile is approximately 0.00024, which means that the averaged freeboard decreases by 2.4 m every 10 km along the ice flow direction. This coincides with the basic knowledge that an ice shelf is always thinner at its ice tongue than upstream.

Fig. 8(b) and (c) also shows some fluctuation along the freeboard profiles A, B and C. This may be because during the evolution of ice shelf, crevasses formed on the surface due to differential horizontal or vertical stresses. The ice shelf also interacted with the tide, the ocean water and the wind forces, and many troughs were formed on the bottom face of the ice shelf, which were identified by many studies (Bindschadler, Vaughan, & Vornberger, 2011). Because of the floatation of ice shelf tongue, these bottom troughs should occur in the same location as their corresponding surface crevasses.

## 7. Conclusions

In this study, detailed measurements of the freeboard, area and ice thickness of the disintegrated MIT were conducted for the first time. The method of producing the freeboard map was introduced specifically. The method considers ice flow and ice shelf melting when combining time-series of ICESat/GLAS data because ice flows downstream from the location where it was first observed. This correction is recommended for detecting freeboard change, especially when ice flow data are available. The area of the disintegrated ice tongue was calculated from both optical and radar images, which show almost the same results. This study sets a good example of the proper procedure for extracting

parameters of iceberg from remote sensing and altimetry data for iceberg observation or tracking. However, because of limited altimetry observations data while the iceberg flowed in the circular Antarctic currents, producing a freeboard map of the continued evolution of an iceberg may be difficult. We have shown that we can produce a freeboard map around the time of calving using multi-sourced data. However, the freeboard of the floating iceberg could be extracted even when there is only one track observation of different altimeters over it. Now that ICESat-1 has stopped working, the Ice-Bridge campaign, Cryosat-2 and the forthcoming ICESat-2 may make future iceberg tracking work more feasible.

## Acknowledgments

We are grateful to the Chinese Arctic and Antarctic Administration for its support, the National Snow and Ice Data Center for the free download of the ICESat/GLAS data and USGS for the free use of the Landsat data. This research was partly supported by the China Postdoctoral Science Foundation (Grant nos: 2012M520185, 2013T60077), National Natural Science Foundation of China (Grant no: 41176163), National High Technology Program of China (Grant no: 2009AA12200101), Fundamental Research Fund for the Central University and Center for Sea Level Change (CSLC) of NYU Abu Dhabi (Grant no: G1204). The Ohio State University (OSU) component of the research was partially supported by grants under the NASA's ICESat-2 Science Definition Team grant (No. NNX12A122G), NASA's Geodetic Imaging Program (No. NNX12AQ07G), and by the Chinese Academy of Sciences/SAFEA International Partnership Program for Creative Research Teams (Grant No. KZZD-EW-TZ-05).

## References

Abshire, J. B., Sun, X., Riris, H., Sirota, J. M., McGarry, J. F., Palm, S., et al. (2005). Geoscience Laser Altimeter System (GLAS) on the ICESat Mission: On-orbit measurement performance. *Geophysical Research Letters*, *32*, L21S02, http://dx.doi.org/10.1029/2005GL024028.

Allison, I., Alley, R., Fricker, H., Thomas, R., & Warner, R. (2009). Ice sheet mass balance and sea level. *Antarctic Science*, *21*(5), 413–426, http://dx.doi.org/10.1017/S0954102009990137.

Alley, R. B., Clark, P. U., Huybrechts, P., & Joughin, I. (2005). Ice-sheet and sea-level changes. *Science*, *310*(5747), 456–460.

Ardhuin, F., Tournadre, J., Queffeulou, P., Girard-Ardhuin, F., & Collard, F. (2011). Observation and parameterization of small icebergs: Drifting breakwaters in the southern ocean. *Ocean Modelling*, *39*(3), 405–410.

Arrigo, K. R., & van Dijken, G. L. (2003). Impact of iceberg C-19 on Ross Sea primary production. *Geophysical Research Letters*, *30*(16), 1836, http://dx.doi.org/10.1029/2003GL017721.

Arrigo, K. R., van Dijken, G. L., Ainley, D.G., Fahnestock, M.A., & Markus, T. (2002). Ecological impact of a large Antarctic iceberg. *Geophysical Research Letters*, *29*(7), 1104, http://dx.doi.org/10.1029/2001GL014160.

Arvidson, T., Gasch, J., & Goward, S. N. (2001). Landsat 7's long-term acquisition plan—An innovative approach to building a global imagery archive. *Remote Sensing of Environment*, *78*(1), 13–26.

Berthier, E., Raup, B., & Scambos, T. (2003). New velocity map and mass-balance estimate of Mertz Glacier, East Antarctica, derived from Landsat sequential imagery. *Journal of Glaciology*, *49* (18-2).

Bindschadler, R. A. (2002). History of lower Pine Island Glacier, West Antarctica, from Landsat imagery. *Journal of Glaciology*, *48*(163), 536–544.

Bindschadler, R., Vaughan, D.G., & Vornberger, P. (2011). Variability of basal melt beneath the Pine Island Glacier ice shelf, West Antarctica. *Journal of Glaciology*, *57*(104), 581–595.

Cook, A. J., & Vaughan, D. G. (2010). Overview of areal changes of the ice shelves on the Antarctic Peninsula over the past 50 years. *The Cryosphere*, *4*(1), 77–98.

Farrell, S. L., McAdoo, D. C., Laxon, S. W., Zwally, H. J., Yi, D., Ridout, A., et al. (2012). Mean dynamic topography of the Arctic Ocean. *Geophysical Research Letters*, *39*, L01601, http://dx.doi.org/10.1029/2011GL050052.

Farrell, S. L., Laxon, S. W., McAdoo, D. C., Yi, D., & Zwally, H. J. (2009). Five years of Arctic sea ice freeboard measurements from the ice, cloud and land elevation satellite. *Journal of Geophysical Research*, *114*, C04008, http://dx.doi.org/10.1029/2008JC005074.

Forsberg, R., & Skourup, H. (2005). Arctic Ocean gravity, geoid and sea ice freeboard heights from ICESat and GRACE. *Geophysical Research Letters*, *32*, L21502, http://dx.doi.org/10.1029/2005GL023711.

Fricker, H. A., Young, N. W., Allison, I., & Coleman, R. (2002). Iceberg calving from the Amery ice shelf, East Antarctica. *Annals of Glaciology*, *34*(1), 241–246.

Heritage, G. L., Milan, D. J., Large, A.R. G., & Fuller, I. C. (2009). Influence of survey strategy and interpolation model on DEM quality. *Geomorphology*, *112*(3–4), 334–344.

Kurtz, N. T., Markus, T., Cavalieri, D. J., Krabill, W., Sonntag, J. G., & Miller, J. (2008). Comparison of ICESat data with airborne laser altimeter measurements over Arctic sea ice. *IEEE Transactions on Geoscience and Remote Sensing*, *46*, 1913–1924.

Kwok, R., & Cunningham, G. F. (2008). ICESat over Arctic sea ice: Estimation of snow depth and ice thickness. *Journal of Geophysical Research*, *113*, C08010, http://dx.doi.org/10.1029/2008JC004753.

Kwok, R., Cunningham, G. F., Zwally, H. J., & Yi, D. (2006). ICESat over Arctic sea ice: Interpretation of altimetric and reflectivity profiles. *Journal of Geophysical Research*, *111*, C06006, http://dx.doi.org/10.1029/2005JC003175.

Kwok, R., Cunningham, G. F., Zwally, H. J., & Yi, D. (2007). Ice, Cloud, and land Elevation Satellite (ICESat) over Arctic sea ice: Retrieval of freeboard. *Journal of Geophysical Research*, *112*, C12013, http://dx.doi.org/10.1029/2006JC003978.

Laxon, S. W., Giles, K. A., Ridout, A. L., Wingham, D. J., Willatt, R., Cullen, R., et al. (2013). CryoSat-2 estimates of Arctic sea ice thickness and volume. *Geophysical Research Letters*, *40*, 732–737.

Laxon, S. W., Peacock, N., & Smith, D. (2003). High interannual variability of sea ice thickness in the Arctic region. *Nature*, *425*(6961), 947–950.

Legresy, B., Wendt, A., Tabacco, I. E., Remy, F., & Dietrich, R. (2004). Influence of tides and tidal current on Mertz Glacier, Antarctica. *Journal of Glaciology*, *50*(170), 427–435.

Lescarmontier, L., Legresy, B., Coleman, R., Perosanz, F., Mayet, C., & Testut, L. (2012). Vibrations of Mertz Glacier ice tongue, East Antarctica. *Journal of Glaciology*, *58*(210), 665–676, http://dx.doi.org/10.3189/2012JoG11J089.

Lin, H., Rauschenberg, S., Hexel, C. R., Shaw, T. J., & Twining, B.S. (2011). Free-drifting icebergs as sources of iron to the Weddell Sea. *Deep Sea Research Part II: Topical Studies in Oceanography*, *58*(11), 1392–1406.

Løset, S., & Carstens, T. (1996). Sea ice and iceberg observations in the western Barents Sea in 1987. *Cold Regions Science and Technology*, *24*(4), 323–340.

Massom, R. A., Hill, K. L., Lytle, V. I., Worby, A. P., Paget, M. J., & Allison, I. (2001). Effects of regional fast-ice and iceberg distributions on the behaviour of the Mertz Glacier polynya, East Antarctica. *Annual of Glaciology*, *33*, 391–398.

Massom, R. A., Giles, A.B., Fricker, H. A., Warner, R. C., Legrésy, B., Hyland, G., et al. (2010). Examining the interaction between multi-year landfast sea ice and the Mertz Glacier Tongue, East Antarctica: Another factor in ice sheet stability? *Journal of Geophysical Research*, *115*, C12027, http://dx.doi.org/10.1029/2009JC006083.

Martin, S., Drucker, R. S., & Kwok, R. (2007). The areas and ice production of the western and central Ross Sea polynyas, 1992–2002, and their relation to the B-15 and C-19 iceberg events of 2000 and 2002. *Journal of Marine Systems*, *68*(1), 201–214.

Martin, T., & Adcroft, A. (2010). Parameterizing the fresh-water flux from land ice to ocean with interactive icebergs in a coupled climate model. *Ocean Modelling*, *34*(3), 111–124.

Maxwell, S. K., Schmidt, G. L., & Storey, J. C. (2007). A multi-scale segmentation approach to filling gaps in Landsat ETM + SLC-off images. *International Journal of Remote Sensing*, *28*(23), 5339–5356.

McMullen, K., Domack, E., Leventer, A., Olson, C., Dunbar, R., & Brachfeld, S. (2006). Glacial morphology and sediment formation in the Mertz Trough. East Antarctica. *Palaeogeography, Palaeoclimatology, Palaeoecology*, *231*, 169–180.

Mueller, T. G., Pusuluri, N.B., Mathias, K. K., Cornelius, P. L., Barnhisel, R. I., & Shearer, S. A. (2004). Map quality for ordinary kriging and inverse distance weighted interpolation. *Soil Science Society of America Journal*, *68*, 2042–2047.

Paul, F., Barrand, N., Berthier, E., Bolch, T., Casey, K., Frey, H., et al. (2013). On the accuracy of glacier outlines derived from remote sensing data. *Annual of Glaciology*, *54*(63), 171–182.

Phillips, H. A., Ridgway, J. R., Minster, J. B., Yi, D. H., & Bentley, C. (1999). *GLAS ATBD-tidal corrections*.

Pyper, W., Rintoul, S., Tilbrook, B., & van Wijk, E. (2011). Mertz glacier calving provides scientific opportunities. *Australian Antarctic Magazine*, *20*, 1.

Rignot, E., & Jacobs, S. S. (2002). Rapid bottom melting widespread near Antarctic Ice Sheet grounding lines. *Science*, *296*, 2020–2023.

Rignot, E., Mouginot, J., & Scheuchl, B. (2011). Ice flow of Antarctic ice sheet. *Science*, *333*(6048), 1427–1430, http://dx.doi.org/10.1126/science.1208336.

Roberts, A., Allison, I., & Lytle, V. I. (2001). Sensible-and latent-heat-flux estimates over the Mertz Glacier polynya, East Antarctica, from in-flight measurements. *Annals of Glaciology*, *33*(1), 377–384.

Scambos, T., Sergienko, O., Sargent, A., MacAyeal, D., & Fastook, J. (2005). ICESat profiles of tabular iceberg margins and iceberg breakup at low latitudes. *Geophysics Research Letters*, *32*(23), L23S09, http://dx.doi.org/10.1029/2005GL023802.

Scambos, T., Fricker, H. A., Liu, C. C., Bohlander, J., Fasttook, J., Sargent, A., et al. (2009). Ice shelf disintegration by plate bending and hydro-fracture: Satellite observations and model results of the 2008 Wilkins ice shelf break-ups. *Earth and Planetary Science Letters*, *280*(1–4), 51–60, http://dx.doi.org/10.1016/j.epsl.2008.12.027.

Scambos, T. A., Hulbe, C., Fahnestock, M., & Bohlander, J. (2000). The link between climate warming and break-up of ice shelves in the Antarctic Peninsula. *Journal of Glaciology*, *46*(154), 516–530, http://dx.doi.org/10.3189/172756500781833043.

Scheuchl, B., Flett, D., Caves, R., & Cumming, I. (2004). Potential of RADARSAT-2 data for operational sea ice monitoring. *Canadian Journal of Remote Sensing*, *30*(3), 448–461.

Schutz, B. E., Zwally, H. J., Shuman, C. A., Hancock, D., & DiMarzio, J. P. (2005). Overview of the ICESat Mission. *Geophysical Research Letters*, *32*, L21S01, http://dx.doi.org/10.1029/2005GL024009.

Schwarz, J. N., & Schodlok, M. P. (2009). Impact of drifting icebergs on surface phytoplankton biomass in the Southern Ocean: Ocean colour remote sensing and in situ iceberg tracking. *Deep Sea Research Part I: Oceanographic Research Papers*, *56*(10), 1727–1741.

Shuman, C. A., Zwally, H. J., Schutz, B. E., Brenner, A.C., DiMarzio, J. P., Suchdeo, V. P., et al. (2006). ICESat Antarctic elevation data: Preliminary precision and accuracy assessment. *Geophysical Research Letters*, *33*, L07501, http://dx.doi.org/10.1029/2005GL025227.

Silva, T. A., & Bigg, G. R. (2005). Computer-based identification and tracking of Antarctic icebergs in SAR images. *Remote Sensing of Environment*, *94*(3), 287–297.

Smith, K. L., Jr., Sherman, A.D., Shaw, T. J., Murray, A. E., Vernet, M., & Cefarelli, A. O. (2011). Carbon export associated with free-drifting icebergs in the Southern Ocean. *Deep Sea Research Part II: Topical Studies in Oceanography*, *58*(11), 1485–1496.

Stuart, K. M., & Long, D.G. (2011). Tracking large tabular icebergs using the SeaWinds Ku-band microwave scatterometer. *Deep-Sea Research Part II*, *58*(11–12), 1285–1300, http://dx.doi.org/10.1016/j.dsr2.2010.11.004.

Tamura, T., Williams, G. D., Fraser, A.D., & Ohshima, K. I. (2012). Potential regime shift in decreased sea ice production after the Mertz Glacier calving. *Nature Communication*, *3*, 826.

Vernet, M., Sines, K., Chakos, D., Cefarelli, A. O., & Ekern, L. (2011). Impacts on phytoplankton dynamics by free-drifting icebergs in the NW Weddell Sea. *Deep Sea Research Part II: Topical Studies in Oceanography*, *58*(11), 1422–1435.

Wang, X. W. (2012). *Applications of ICESat/GLAS data in elevation change studies.* Ph.D Thesis. Beijing, China: Institute of Remote Sensing Applications, Chinese Academy of Sciences.

Wang, X. W., Cheng, X., Gong, P., Huang, H. B., Li, Z., & Li, X. W. (2011). Earth Science applications of ICESat/GLAS: A review. *International Journal of Remote Sensing*, *32*(23), 8837–8864, http://dx.doi.org/10.1080/01431161.2010.547533.

Wang, X. W., Cheng, X., Huang, H. B., & Li, Z. (2013). DEM generation in dome-A area with GLAS and GPS data. *Journal of Remote Sensing*, *17*(2), 424–429.

Wang, X. W., Cheng, X., Li, Z., Huang, H. B., Niu, Z. G., Li, X. W., et al. (2012). Lake water footprints identification from time-series ICESat/GLAS data. *IEEE Geoscience and Remote Sensing Letters*, *9*, 3, http://dx.doi.org/10.1109/LGRS.2011.2167495.

Wang, X. W., Gong, P., Zhao, Y., Xu, Y., Cheng, X., Niu, Z., et al. (2013). Large lake water-level changes in China determined from ICESat/GLAS data. *Remote Sensing of Environment*, *132*(C), 131–144, http://dx.doi.org/10.1016/j.rse.2013.01.005.

Wendler, G., Ahlnas, K., & Lingle, C. S. (1996). On Mertz and Ninnis Glaciers, East Antarctica. *Journal of Glaciology*, *42*(142), 447–453.

Yi, D., Zwally, H. J., & Robbins, J. (2011). ICESat observations of seasonal and interannual variations of sea-ice freeboard and estimated thickness in the Weddell Sea, Antarctica (2003–2009). *Annals of Glaciology*, *52*(57), 43–51.

Zhao, Z. Y., Liu, Z., & Gong, P. (2012). Automatic extraction of floating ice at Antarctic continental margin from remotely sensed imagery using object-based segmentation. *Science China Earth Sciences*, *55*(4), 622–632.

Zwally, H. J., Schutz, B., Abdalati, W., Abshire, J., Bentley, C., Brenner, A., et al. (2002). ICESat's laser measurements of polar ice, atmosphere, ocean, and land. *Journal of Geodynamics*, *34*, 405–445.

Zwally, H. J., Giovinetto, M. B., Li, J., Cornejo, H. G., Beckley, M.A., Brenner, A.C., et al. (2005). Mass changes of the Greenland and Antarctic ice sheets and ice shelves and contributions to sea level rise: 1992–2002. *Journal of Glaciology*, *51*(175), 509–527.

Zwally, H. J., Yi, D., Kwok, R., & Zhao, Y. (2008). ICESat measurements of sea ice freeboard and estimates of sea ice thickness in the Weddell Sea. *Journal of Geophysical Research*, *113*, C02S15, http://dx.doi.org/10.1029/2007JC004284.